Journal of Molecular Graphics and Modelling 27 (2009) 969–977

Contents lists available at ScienceDirect

Journal of Molecular Graphics and Modelling

journal homepage: www.elsevier.com/locate/JMGM

Computational screening and design of S100B ligand to block S100B–p53 interaction

John L. Whitlow [a], Jayson F. Varughese [a], Zhigang Zhou [b], Libero J. Bartolotti [a], Yumin Li [a,*]

[a] Department of Chemistry, East Carolina University, Greenville, NC 27858, United States
[b] Department of Medicinal Chemistry and Molecular Pharmacology, Purdue University, West Lafayette, IN 47907, United States

ARTICLE INFO

Article history:
Received 31 December 2008
Received in revised form 10 February 2009
Accepted 11 February 2009
Available online 20 February 2009

Keywords:
S100B
p53 tumor suppressor
Virtual screening
Molecular dynamics simulation
Binding affinity

ABSTRACT

The binding of S100B to p53 disables the biological function of p53 as a tumor suppressor and thus causes cancer. It is very important to explore the interaction between S100B and p53 and to develop inhibitors to block the interaction in anti-cancer development. In this work, the interaction of S100B to p53 was studied using molecular dynamics (MD) at the atomic level and organic molecules have been identified as potential inhibitors to block the S100B–p53 interaction. It was indicated in the simulations that S100B residues around GLU45 and GLU46 play an important role in the binding of S100B to p53. The three dimensional structure of S100B obtained from S100B–p53 complex (PDB ID: 1DT7) was used as the target protein receptor. Multiple LUDI screenings for S100B ligands were performed using different searching radii 6.23 Å, 7.23 Å, 8.23 Å, 9.23 Å and 10.23 Å with a searching center which was defined as the geometrical center of S100B residues that are within 5 Å from the p53 C-terminal peptide in the complex. Potential organic compounds were screened from the ZINC database using LUDI program implemented in Cerius2 package and evaluated as potential S100B ligands to block the S100B–p53 interaction. The top-scored compounds were selected for binding affinity calculation. The results show that these top-scored ZINC compounds bind in the location where p53 binds and interact with S100B in a similar fashion as p53, and therefore it is expected that they have the potential to block S100B from binding to p53. The ADME and toxicity properties of the potential S100B ligands were also evaluated.

1. Introduction

S100 proteins are a family of dimeric EF-hand Ca^{2+} binding proteins and have been implicated in a wide range of biologically important signaling pathways [1–3]. Overexpression of S100 proteins has been associated with a spectrum of human diseases including cardiomyopathies, neurodegeneration, and cancer [4,5]. S100B is the prototype of S100 family and is primarily found in glial cells and has been associated with the Alzheimer's disease, Down's syndrome and several forms of cancers [2,3,6,7]. More than 20 target proteins of S100B have been identified including the Alzheimer protein tau [8,9], neuromodulin [10] and tumor suppressor protein p53 [11], etc. p53 is a transcriptional activator, which is frequently referred to as "The Guardian of the Genome" due to its tumor suppressing activities. In cells, p53 tetramer is required for p53 to adequately function [12,13]. p53 in the tetrameric form can stop the cell cycle, prevent genetic alterations, and induce apoptosis in response to the activation of certain oncogenes [14,15]. Experimentally it was observed that S100B binds to the lower oligomerization states (monomer or dimer) of tumor suppressor p53 [11,16–18]. Such binding disrupts the tetramerization equilibrium of p53 and prevents p53 from functioning and thus has been strongly associated with cancer [1,19–26].

Three-dimensional structures of S100B at different biological states including calcium-free state [27], calcium-binding state [28] and p53-binding state [11] have been determined using NMR spectroscopy, which are shown in Fig. 1A–C. S100B exists as a homodimer in solution, and each monomer can bind two calcium ions at the loop regions [28]. Calcium-free S100B does not bind with p53. The binding of S100B with p53 is triggered by calcium. Calcium binding on S100B induces a large conformational change and generates a hydrophobic surface by changing the orientation of helix III and helix IV and placing helix III nearly perpendicular to helix IV and extending the helix IV by one turn so that S100B can interact with p53 and other protein targets inside the cell to regulate their biological functions [28].

The NMR determined three-dimensional structure of the calcium-bound S100B complex with the C-terminal peptide of p53 provides appropriate starting coordinates for the computational investigation of S100B-p53 interaction at atomic resolution, which serves as the key for rational drug design to block the

* Corresponding author. Tel.: +1 252 328 9763; fax: +1 252 328 6210.
E-mail address: liyu@ecu.ecu (Y. Li).

1093-3263/$ – see front matter © 2009 Elsevier Inc. All rights reserved.
doi:10.1016/j.jmgm.2009.02.006

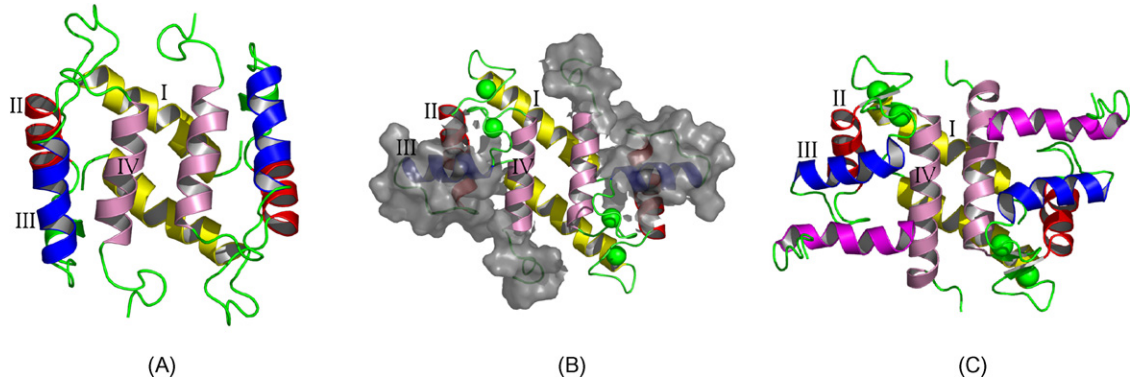

Fig. 1. Ribbon representation of rat-S100B at calcium-free state (A), calcium binding state (B) with the hydrophobic surface for target binding shown in grey, and C-terminal of p53 binding state (C). The calcium ions are indicated as green spheres and p53 C-terminal peptides are in magenta.

cancer-causing interaction. In this work, the S100B–p53 interaction was calculated at an atomic level using molecular dynamics simulation method of the CHARMM program [29] and all-hydrogen CHARMM27 force field [30]. A set of potential S100B-binding ligands were generated using LUDI program [31] implemented in Cerius2 package [32] and ZINC database [33].

2. Methods

2.1. Calculating S100B–p53 interaction

Molecular dynamics simulations were carried out on the three-dimensional structure of S100B complex with the C-terminal peptide of p53 (Fig. 1C, 1DT7.pdb). Since the structure was determined using NMR spectroscopy, the best representative of the NMR ensembles of structure was chosen as the initial structure, which includes 22 residues from C-terminal domain of p53, 184 residues of S100B and four calcium ions. The starting structure was neutralized with counter ions (Cl^-), and explicitly solvated using TIP3P water [34] in an rectangle water box. The total number of the atoms of the simulation system was 56941 including protein and water. The system, including protein and water, was prepared for simulation by energy minimization to remove the bad contacts and was gradually heated to 300 K. Constant pressure (NPT) molecular dynamics (MD) simulation was performed on the equilibrated system for 100 ps. The density of the systems was stabilized around 1 kg/m^3 by the end of NPT simulation. Finally, production MD simulation was performed with constant volume dynamics (NVT) for the system for 10 ns and snapshots were collected from the production simulation for analysis. All the computations including the minimization and MD simulations for S100B–p53 peptide complex were performed using 128 processor Altix4700 IBM and using AMBER's all atom force field as implemented in AMBER9 software [36]. The details of this computation for S100B–p53 complex are the same as that for the S100B–ligand complexes, as described below.

2.2. S100B–ligand binding affinity calculation

2.2.1. Molecular dynamics simulation on the S100B–ligand complexes

Based on the LUDI docking structures, molecular dynamics simulations were performed for S100B complex with each of the 14 compounds; the 14 compounds were selected from the visual examination [35] of top 20 compounds selected from screening results based on LUDI score as listed in Table B of Supplementary materials. The S100B–ligand complexes were neutralized with counter ions (Cl^-), and explicitly solvated using TIP3P water in an octahedral water box. The structures of the 14 ligands were optimized using semi-empirical AM1 method included in MOPAC6 package. The partial charges for the ligands were fitted from the calculated charges using AM1 method though the Antechamber module of AMBER.

All calculations were performed using AMBER's all atom force field as implemented in AMBER9 software [36]. The SANDER module of AMBER program was used for the computation. Simulations were carried out under periodic boundary conditions with a cutoff of 12 Å for the VDW non bonded interactions. The particle-mesh Ewald method [37–40] was used to treat the long-range electrostatic contribution to the force field. The SHAKE algorithm [41] was employed to constrain the hydrogen atoms and allow the usage of longer step size of 2 fs.

All the systems were energy minimized before each MD simulation. A restrained minimization was first performed on solvent while keeping S100B and the ligand fixed; then the entire system was minimized. The minimized systems were warmed for 20 ps to a final temperature of 300 K. Constant pressure dynamics (NPT) was performed on the warmed system for 100 ps. During this step, the density of the systems was stabilized to 1. Finally, constant volume dynamics (NVT) was performed.

2.2.2. S100B–ligand binding affinity calculation using MMPBSA

The binding affinity of ligand to the interface of S100B protein with p53 was analyzed by the Molecular Mechanics Poisson–Boltzmann Surface Area (MMPBSA) method [42–44], integrated in AMBER9 [36]. The binding affinity measured in terms of free energy of binding was calculated as the average of the binding free energy of the last 250 snapshots, taken at 15 ps intervals from the trajectories of each simulation of 7.5 ns. The free energy was calculated as:

$$\Delta G_{\text{tot}} = \Delta E_{\text{MM}} + \Delta G_{\text{sol}} - T\Delta S \quad (1)$$

where ΔE_{MM} is the molecular mechanics energy base on AMBER force field, consisting of a vander Waals and an electrostatic energy; ΔG_{sol} is the solvation energy, including electrostatic and nonpolar interactions. The electrostatic part of solvation energy is calculated using the Poisson–Boltzmann method and the nonpolar contribution is estimated by the solvent-accessibility surface method. $T\Delta S$ is the entropy contribution to the free energy and can be estimated using normal mode analysis. The binding affinity can be estimated by the following format:

$$\Delta G_{\text{b}} = \Delta G_{\text{c}} - (\Delta G_{\text{p}} + \Delta G_{\text{l}}) \quad (2)$$

Where c, p and l denote the protein/ligand complex, the protein and the ligand, respectively.

2.3. LUDI screening for potential S100B–binding ligand

2.3.1. LUDI virtual screening

The LUDI program implemented in the Accelrys Cerius2 package was used for S100B ligand screening. LUDI operates in three distinct steps. The first step is to generate the interaction sites for the defined receptor binding site. Then the compound database is screened for hits that fit the interaction sites. Finally, an alignment or linking is created for compound using the Kabsch algorithm [45].

2.3.2. Protein receptor and center of searching

To generate S100B ligands with the aim to block p53 interaction using the LUDI program, a protein receptor and the binding site need be defined prior to the LUDI screening. Binding of a ligand to S100B at the same location as p53 binds will block the S100B–p53 interaction. The S100B protein taken from S100b–p53 complex by removing p53 was used as target protein for screening. The binding site of p53 on S100B was used as screening site.

The screening sites were defined by selecting all the amino acids of S100B which are 5 Å around p53. The geometrical center of these selected S100B resides was used as the searching center in the ligand screening. This was done using the Active Site Viewer module within Cerius2. The searching center and the searching radius together define the searching site. In this work, five different searching radii (6.23 Å, 7.23 Å, 8.23 Å, 9.23 Å and 10.23 Å) were used in the LUDI screening.

2.3.3. The options used in LUDI screening

The "Receptor Based Design" module within LUDI was used to screen ZINC compounds for molecules with high affinities within the defined S100B active site. The resultant list of compounds was scored and ranked by hydrogen bond score, number of hydrogen bonds, ionic bonds, lipo score, aromatic score, contact, link score, and RMS deviation. Compounds had to have a 2.50 Å minimum distance separating a polar hydrogen in the compound from a polar hydrogen in the receptor, and were subject to an electrostatic check. The more thorough "Best" search option was used over the "Fast" option even though test runs have shown that both options find the exact same molecules and take almost the same amount of time. The only difference detected in the log files was that the "Best" option, in a few instances, performed slightly more rotations of the molecules than the "Fast" option indicating why it took slightly longer to complete. However, in all cases the final results were the same. For the LUDI screenings performed in this work, the software was configured to allow one rotable bond at a time.

2.3.4. Small molecule database

Irwin and Shoichet's ZINC database version 2005 was used in this work. The ZINC "drug like" set, containing 2.6 million drug-like compounds, was screened for S100B ligand. In the ZINC "drug like" set, the following molecules have been prescreened and removed based on "Rule of 5" [46], log P greater than 5 and less than 4, hydrogen bond donors greater than 5, hydrogen bond acceptors greater than 10, number of rotable bonds greater than 15, all molecules containing atoms other than H, C, N, O, F, S, P, Cl, Br, or I. All molecules in this database are compounds readily available from major chemical supply vendors. The database is thoroughly annotated, and can be screened for functional groups, molecular weight, calculated log P, protonation state, tautomeric form, stereochemistry, and isomers.

In order to use ZINC "drug-like" set in LUDI screening, the ZINC structure data format (SDF) was converted to create two files, one is the structure file including the topological information with the extension ".str", and another is the target file (extension .trg) that contains the interaction types of each molecule's functional groups. This was done using "genlib" command within LUDI program.

2.4. ADMET prediction

Most of drug failures are due to ADME (absorption, distribution, metabolism and excretion) and toxicity problems. To prevent wasting time on lead candidates that would be toxic or metabolized by the body into an inactive form and unable to cross membranes, the potential ligands generated using LUDI were screened using ADMET Predictor [47]. ADMET Predictor uses mathematical models built on available drug information to quantitatively predict properties for organic molecules. The program calculates molecular descriptor values for each structure loaded into the program and then uses these values as inputs for the different models to estimate a certain property.

ADMET Predictor has a set of rules (Table 1) that specify a threshold for each model-based property. Any compound that does not satisfy a rule was assigned a TOX hit of 1 for each independent property. For example, the S + Sw rule assigns a value of 1 to ZINC01812405 since the predicted value falls below 8×10^{-3} mg/ml suggesting that the compound may be less soluble in the body. The Admet-risk column in Table 1 is a sum of the TOX hits for each compound. A higher number in the Admet-risk column signifies a greater probability that the drug may fail in clinical trials.

Our group mainly focused on 6 ADME models and 5 Toxicity models to predict different drug characteristics. The 6 ADME models were used to predict hydrophobicity, solubility and permeability. The Mlog P model is a predictor for the ratio of the concentration of a compound in octanol and water. This model was built using a database of 1230 compounds and relates to the hydrophobicity of the drug [48]. The S + Peff model predicts human jejunum effective permeability based on in vivo permeability values from human subjects and reflects the transport velocity across the epithelial barrier in the intestine [49]. The S + Sw model predicts the saturated concentration of a pure neutral compound in water [50]. The S + BBB model uses a data set of 230 chiral-specific compounds and provides insight to the permeability of the drug through the blood-brain barrier [51]. A value of "high" predicted by S + BBB model denotes easy permeation and a value of "low" indicates poor permeation according to the study by Crivori et al. The percent of drug that remains free in blood plasma is characterized by the S + PrUnbnd model which is built on experimental data of 331 drugs. The S + Vd model was built based on 370 characterized drug data and predicts the volume of distribution utilized in the pharmokinetics of a drug.

In addition to absorption and permeation, Admet Predictor provides 5 models to predict toxicity based on quantitative structure-activity relationships (QSAR). The TOX-ER model focuses on the potential of drugs to bind with the estrogen receptor causing disruptions in the endocrine system. This model is based on a study involving 230 chemicals, including natural estrogens

Table 1
ADMET rules.

Column	Property	Rule	Tox hit
A	BRM-SAL	"Positive"	1
B	MlogP	<−0.590	1
C	S + Peff	<0.864 cm/s	1
D	S + Sw	<8e−3 mg/mL	1
E	S + BBB	"Low"	1
F	S + PrUnbnd	<1%	1
G	S + Vd	>15 L/kg	1
H	MRTD	<2.7 mg/kg/day	1
I	TOX-ER	>0.038	1
J	TOX-FHM	<22.8 mg/L	1
K	BRM_RAT	<14.8 mg/kg/day	1

and xenoestrogens, and predicts the relative binding affinity ratio of estrogen binding over the drug in question [52]. The TOX–FHM model is based on DSSTox database, compiled by U.S. Environmental Protection Agency, with 577 compounds and involves the lethal effects of drugs on 50% of the fathead minnow (Pimephales Promelas) population during a 96 h exposure time [53,54]. Mutagenicity and carcinogenicity are represented by the BRM-SAL and BRM-RAT modelss, respectively. The Salmonella model utilizes the DSSTox database with a total of 506 compounds and the model yields a "positive" or "negative" value to describe the possibility of mutagenicity with a certain drug [54,55]. The rat carcinogenicity model is built using data from long-term carcinogenic bioassays in the Carcinogenic potency database (CPDB) and predicts the dose (TD_{50} value) administered over a lifetime that results in the appearance of tumors in 50% of the population [56]. Furthermore, the program also provided the means to investigate the maximum therapeutic dose through the TOX-MRTD model. This model is based on a database compiled by the US Food and Drug Administration organization consisting of 1181 drugs [57].

3. Results and discussion

3.1. S100B–p53 interaction from MD simulations

The root mean square coordinate deviations (RMSD) of the system with and without p53 C-terminal peptides were calculated and the results are included in Fig. 2, which demonstrated that in the complex of S100B and p53 C-terminal peptide, the p53 C-terminal peptide is very flexible (upper plot), while the S100B structure is very stable (lower plot). A possible explanation of the flexibility of p53 chain in the simulation may be that the C-terminal peptide (11 amino acids) is only a small fraction of the complete p53 protein and therefore it is not structurally stable. It is also noticed that the helical structure of p53 C-terminal peptide of 11 amino acids gradually loses its secondary structure during simulation. Therefore, the minimized structure from experimental complex was used to explore the interaction of S100B with p53. The calculated results are plotted in top panel of Fig. 3. The green plot shows that the electrostatic interaction is the dominant energy in the binding of S100B with p53; the red plot shows that the VDW interaction of S100B and p53 is weak; the black plot is the total interaction energy including vander Waals energy and electrostatic energy. It can be seen from the top panel of Fig. 3 that the residues of S100B interacting with p53 are in the regions

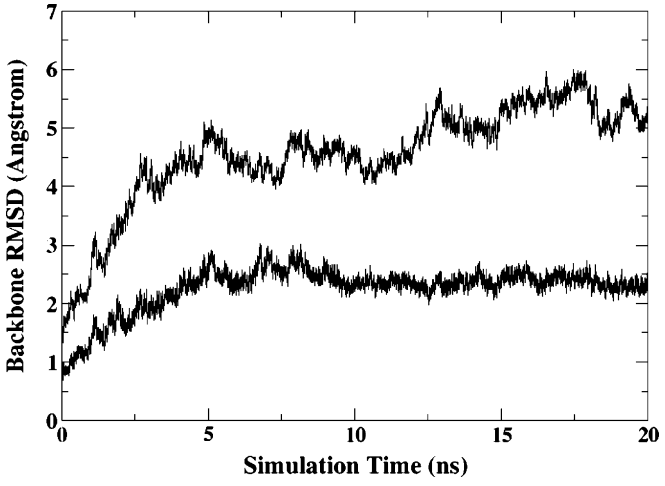

Fig. 2. The backbone RMSD (in Å) of S100B complex with C-terminal peptide of p53 (upper plot) included, and with the C-terminal peptide of p53 excluded (lower plot).

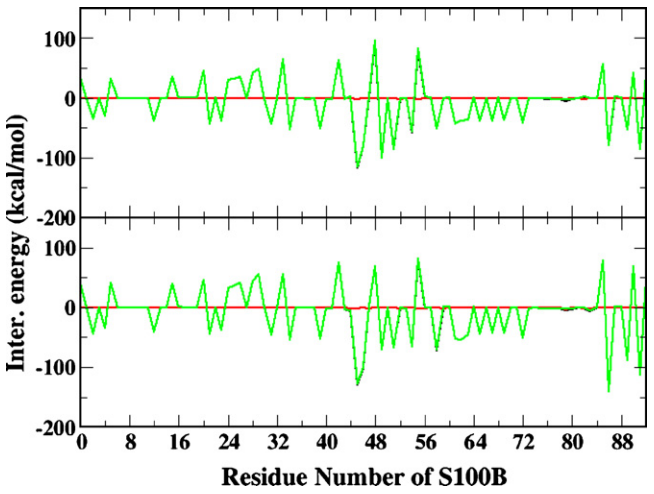

Fig. 3. The interaction energy of p53 C-terminal peptide with each residue of S100B calculated at the minimized structure (upper panel) and calculated using MMPBSA approach based on the AMBER simulation trajectory (lower panel). The green plots indicate the electrostatic interaction; and the red plots indicate the VDW interaction.

from 44 to 59 and from 86 to 90. Among all the S100B residues GLU45 and GLU46 have the strongest interaction with p53. In addition, the S100B–p53 interaction was calculated using MMPBSA approach based on the simulation. The results are shown in Fig. 3 lower panel, which indicates that in addition to residues around GLU45 and GLU46, C-terminal residues of S100B have also interaction with p53.

Besides, the molecular dynamics simulation was also carried out for this complex of S100B with the C-terminal domain of p53 using CHARMM [29,30]. The consistent results were obtained.

3.2. LUDI screening with radius 6.23 Å, 7.23 Å, 8.23 Å, 9.23 Å and 10.23 Å, respectively

As detailed in the computational method, the searching target protein was S100B taken from S100B–p53 complex (PDB ID: 1DT7) and the searching center was defined as the geometrical center of S100B resides within 5 Å away from the p53 peptide in the S100B–p53 complex (PDB ID: 1DT7). Multiple LUDI screenings were performed using different searching radius 6.23 Å, 7.23 Å, 8.23 Å, 9.23 Å and 10.23 Å. Using the receptor based model, the ZINC "drug-like" compounds were fitted on the interaction sites to identify the molecules (hits) which have the potential to bind S100B and block p53 from binding to the S100B protein. The ZINC "drug-like" compounds were scored based on their interactions with S100B at the defined binding site. All the ZINC "drug-like" compounds with the LUDI score of 300 or above are listed in the Table A of Supplementary materials.

It is seen in Table A of Supplementary materials that the number of compounds with a LUDI score of 300 or above obtained from LUDI screening against the S100B binding site increases as the radius of searching increases. At the smallest radius of 6.23 Å, 23 compounds from the Zinc database were found. At 7.23 Å, 90 compounds were found. This trend that the number of hits increases with the increase of searching radius continues with the radius of 8.23 Å, 9.23 Å, and 10.23 Å which generate 138 compounds, 251 compounds, and 370 compounds, respectively. The LUDI algorithms seem to be fairly deterministic with consistent repeatable results, even with increasing radius. In other words, compounds found at smaller radii were retained in the search results of larger radii. For example, the compound ZINC03307740 is ranked best in multiple LUDI screenings with radius of searching (7.23 Å, 8.23 Å and 9.23 Å, 10.23 Å). As the

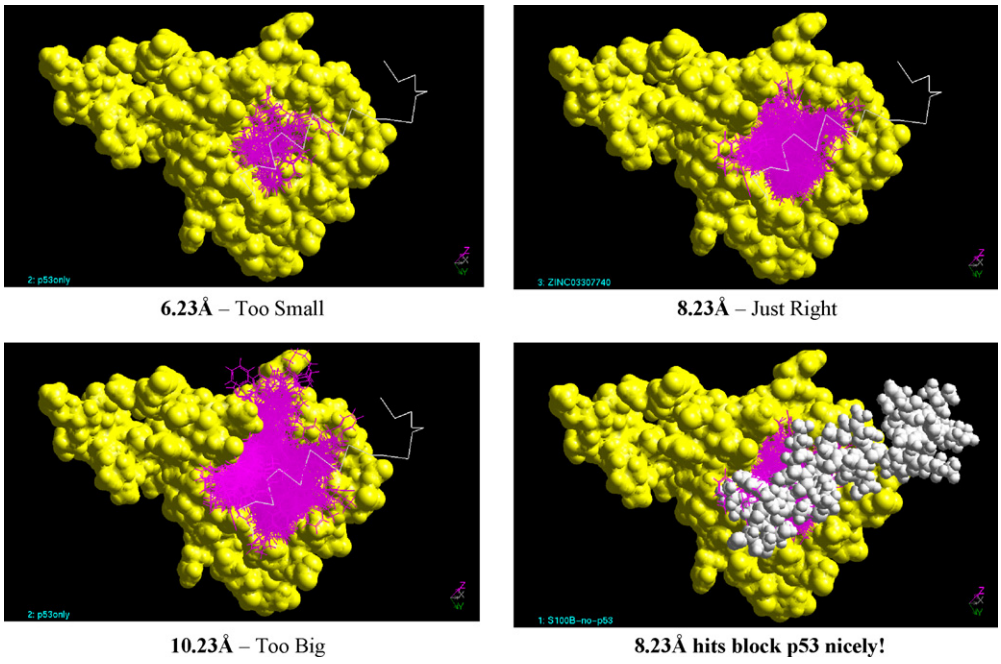

Fig. 4. Determining the searching radius. S100B is in yellow, hits in magenta, and p53 C-terminal peptide in grey.

radius increased, additional interaction sites were created which allowed additional hits. The compound ZINC01814105 was ranked No.1 with radius of searching 6.23 Å, No.2 with radius of searching 7.23 Å, No.3 with radius of searching 8.23 Å, No.4 with radius of searching 9.23 Å, and No.5 with radius of searching 10.23 Å. There were a few exceptions to this repeatability trend.

The binding structures of all ZINC compounds with LUDI score of 300 or above listed in Table A of Supplementary materials in the binding site of S100B were aligned in Fig. 4. It seems that the hits from one specific search nearly occupy all the area of the defined binding site in the same search. Clearly the larger the radius of searching, the more hits from ZINC compounds were found. However it is also noticed that if the searching radius (6.23 Å) is too small, the search may not explore all possible area where p53 contacts with S100B. While, if the searching radius (10.23 Å) is too large, the molecules may bind outside of the area where p53 contacts with S100B. Such ligand binding will have low potential to block the p53 from binding to S100B. Thus the optimum searching radius based on these observations is apparently 8.23 Å. Therefore further analyses on the interactions and the ADME properties were focused on the hits generated from the LUDI run with the searching radius of 8.23 Å.

3.3. S100B–ligand interaction

To further analyze the binding and interaction of these newly generated compounds with S100B protein receptor to facilitate the generation of a pharmacophore model for new design, the interaction details at an atomic level including hydrogen bond interaction and hydrophobic interaction between each compound and protein receptor S100B were generated and were listed in Table B of Supplementary materials for the compounds generated from the screening with the searching radius of 8.23 Å. As can be seen from Table B of Supplementary materials, the screened ZINC "drug-like" compounds may interact with S100B at residues GLU45, GLU46, LEU44, VAL52, LYS55, VAL56, THR59, PHE76, MET79, VAL80, ALA83, PHE87. There are 50 compounds in Table B of Supplementary materials that interact with GLU45, 29 compounds that interact with GLU46, 32 compounds that interact with LEU44, 17 compounds that interact with VAL52, 28 compounds that interact with LYS55, 44 compounds that interact with VAL56, 21 compounds that interact with THR59, 30 compounds that interact with PHE76, 35 compounds that interact with MET79, 25 compounds that interact with VAL80, and 20 compounds that interact with ALA83. The compounds form hydrogen bonds with residues GLU45, GLU46 and MET79, and form hydrophobic interactions with other S100B residues listed above. The binding structures of the four top-scored ZINC compounds (ZINC03307740, ZINC03257333, ZINC01814105 and ZINC00468414) in Table B of Supplementary materials are shown in Fig. 5. The compound, ZINC03307740 and ZINC03257333 form hydrogen bonds with the GLU45 and GLU46. ZINC01814105 and ZINC00468414 form hydrophobic interactions with MET79, and other residues. As described previously in the section of "Method", the most dominant binding sites of S100B–p53 C-terminal peptide interaction lie at the GLU45 and GLU46 and around residues. This indicates that these top-scored ZINC compounds generated from LUDI screening have the potential to bind with S100B at the same binding sites as the C-terminal of p53. Such ligand binding will interfere the binding of p53 to S100B. Therefore, these ZINC compounds are expected to bind with S100B and block the interaction with p53.

3.4. The stability of ligand binding to S100B protein

These putative ligands were screened to bind to S100B at the interface with p53 protein. The important thing for these ligands is to bind to the site with reasonable stability in the normal physiologic condition. MD simulation was used to simulate the interaction of these ligands with the protein receptor to evaluate the binding stability. The contact between the ligands and protein during the 5 ns of MD simulation is measured in terms of the distance between the ligand and protein contact surface. The distance between the center of ligand and that of S100B is depicted in Fig. 6. The plots of distances are roughly flat for the ligands ZINC03307740 (E), ZINC03257333 (D), ZINC00468414 (J), ZINC01014143 (K), ZINC01270855 (L) and ZINC00401150 (H). This indicates that these ligands maintain good contacts with the protein surface and did not fall off from the protein during such long simulation. The phenomenon shows that the binding of these

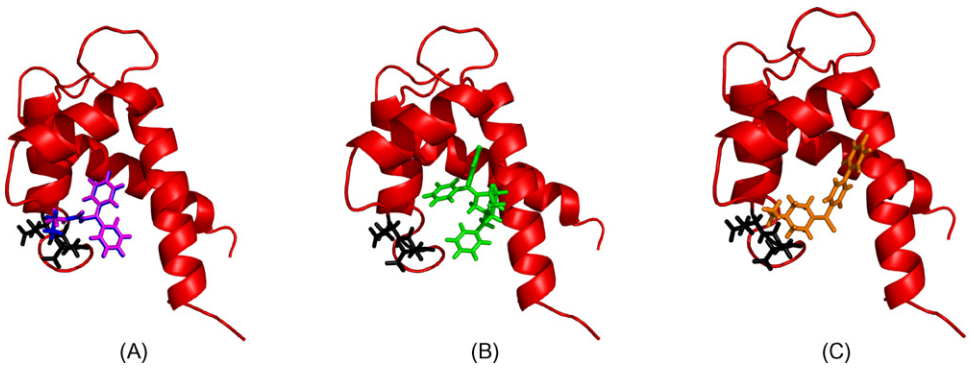

Fig. 5. The alignments of top four ZINC compounds (as sticks) from Table B of Supplementary materials with S100B. The No. 1 and No. 2 compounds are shown in (A), the No.3 compound in (B), and No.4 compound in (C). The GLU45 and GLU46 of S100B are shown as black sticks.

ligands to the protein site is stable. On the other hand, the plots of ligands ZINC01743229 (A), ZINC01398712 (N), ZINC03656567 (F), ZINC02066493 (B) and ZINC01395932 (M) have relatively large fluctuations, especially those of ligands ZINC01398712 (N) and ZINC01743229 (A), which are drifting away from the initial structures. The larger fluctuations on these plots mean that these ligands are more mobile when binding to the pocket by moving on the binding surface. The two ligands ZINC01398712 (N) and ZINC01743229 (A) have problem to bind stably to the binding site.

3.5. Binding affinity calculation

The binding energy of these selected compounds to bind with S100B protein was calculated using MMPBSA method based on the last 250 snapshots taken from 7.5 ns simulation at a 15 ps interval for each ligand/protein complex. This binding energy is a way to measure the binding affinity of ligand and protein interaction, especially to evaluate a relative binding affinity of a set of similar compounds to a protein receptor. The calculated binding energy for the selected ligands with S100B protein is listed in Table 2. It is seen that these compounds have reasonable binding affinity to the protein. The binding energy includes the molecular mechanic energy ($E_{int} + E_{electronic} + E_{vdW}$), the solvation energies from PBSA model, and the entropy contribution from vibration partition to the binding process. The translational and rotational contributions to the entropy change is not included as they are the same to such ligand binding and we are focusing on the comparison of relative binding strength of this set of ligands. The ligand ZINC01014143 (K) has highest binding affinity with a ΔG of −28.02 kcal/mol compared to other compounds while ligand ZINC01395932 (M) has lowest binding with a ΔG of −10.67 affinity to the protein.

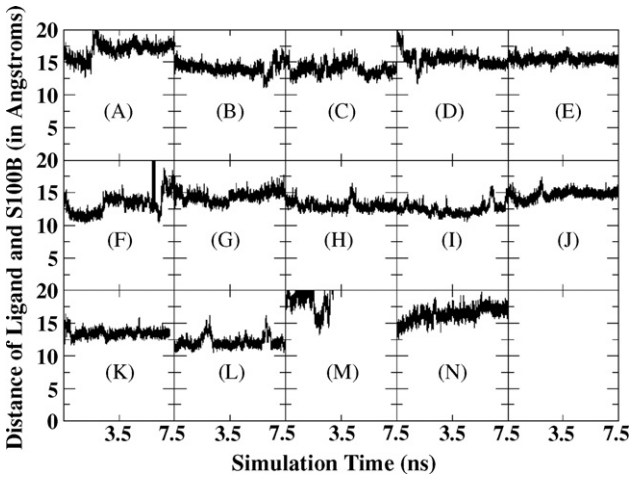

Fig. 6. The distance plots between the center of ligand and the center of S100B protein. Plot (A) is for ZINC01743229, (B) for ZINC02066493, (C) for ZINC02288410, (D) for ZINC0325733, (E) for ZINC03307740, (F) for ZINC03656567, (G) for ZINC00394841, (H) for ZINC00401150, (I) for ZINC00046707, (J) for ZINC00468414, (K) for ZINC01014143, (L) for ZINC01270855, (M) for ZINC01395932 and (N) for ZINC01398712.

It is noticed that the ligands with higher binding energy in the Table 2 have flatter plots on the Fig. 6. It makes sense that if a ligand has favorable interactions with the protein and has a strong binding; it will have higher binding energy and will not move around. On the other hand, the molecules with weaker interactions with the protein will have lower binding energies and possibly move around on the binding surface to locate better sites, or even

Table 2
The calculated binding energy from MMPBSA method based on the last 250 snapshots at a 15 ps interval taken from the trajectories of 7.5 ns simulation for each of complexes.

Ligand	E_{mm}	E_{sol}	$E_{mm} + E_{sol}$	$T\Delta S_{vib}$	ΔG	log K_d
ZINC01014143	−36.95±4.61	14.14 ± 3.04	−22.81 ± 3.10	5.21 ± 4.46	−28.02	−4.9128
ZINC03307740	−36.03 ± 2.78	13.69 ± 2.45	−22.33 ± 2.19	5.5 ± 5.18	−27.83	−4.8795
ZINC02288410	−28.46 ± 3.87	7.56 ± 2.79	−20.91 ± 2.63	4.38 ± 4.10	−25.29	−4.4342
ZINC00401150	−29.85 ± 4.48	11.06 ± 3.28	−18.8 ± 2.24	5.65 ± 6.41	−24.45	−4.2869
ZINC03656567	−31.85 ± 7.13	13.41 ± 3.86	−18.44 ± 4.26	5.77 ± 7.09	−24.21	−4.2448
ZINC00468414	−31.93 ± 3.86	13.16 ± 3.04	−18.78 ± 2.88	4.94 ± 5.52	−23.72	−4.1589
ZINC03257333	−29.86 ± 6.28	12.9 ± 6.11	−16.96 ± 2.58	5.95 ± 4.70	−22.91	−4.0169
ZINC00394841	−28.16 ± 6.74	11.83 ± 5.8	−16.33 ± 2.68	6.56 ± 4.63	−22.89	−4.0134
ZINC01270855	−27.81 ± 3.75	11.34 ± 2.78	−16.47 ± 2.75	5.95 ± 4.69	−22.42	−3.931
ZINC02066493	−25.27 ± 4.78	7.72 ± 3.61	−17.55 ± 2.83	3.47 ± 4.71	−21.02	−3.6855
ZINC01398712	−40.75 ± 5.79	25.03 ± 5.25	−15.72 ± 2.40	5.19 ± 4.85	−20.91	−3.6662
ZINC01743229	−31.8 ± 5.78	15.68 ± 4.62	−16.12 ± 3.78	4.08 ± 3.74	−20.2	−3.5417
ZINC00046707	−26.93 ± 4.66	8.61 ± 4.44	−18.32 ± 3.55	1.55 ± 4.38	−19.87	−3.4839
ZINC01395932	−8.79 ± 10.62	5.67 ± 9.7	−3.12 ± 2.32	7.55 ± 4.92	−10.67	−1.8708

E_{mm} is the molecular mechanics binding energy based on force field, $E_{mm} = E_{int} + E_{eletronic} + E_{vdw}$; E_{sol} is the solvation contribution to the binding energy calculated using PBSA implicit water model; $T\Delta S_{vib}$ is the entropy contribution from the vibration part to the binding estimated based on Normal Mode Analysis; $\Delta G = E_{mm} + E_{sol} - T\Delta S_{vib}$; log $K_d = -\Delta G$.

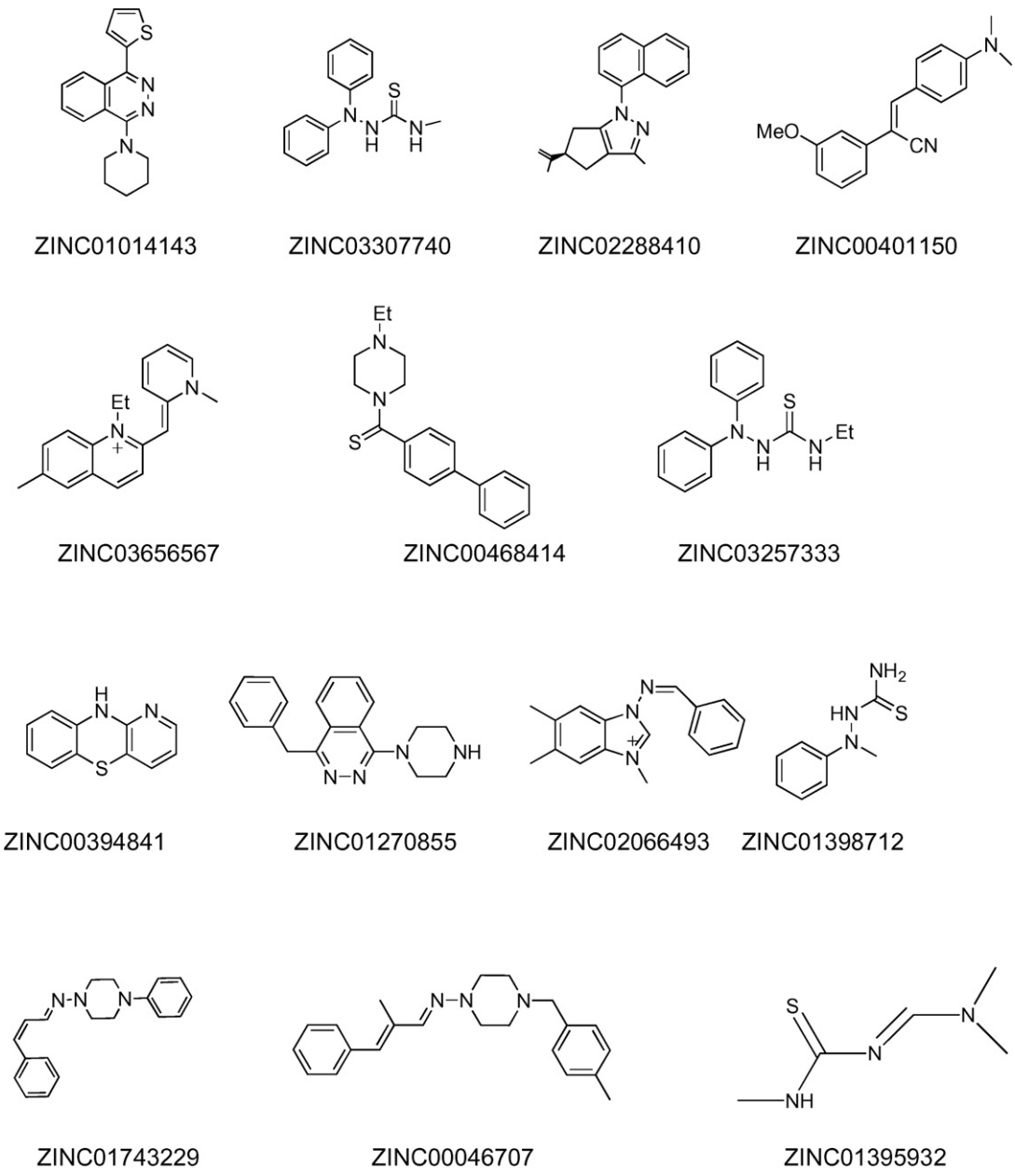

Fig. 7. The 2D structures of compounds listed in Table 2.

flow away from the initial binding site. The 2D structures of these compounds listed in Table 2 are shown in Fig. 7.

3.6. Interaction mode of compound with the protein

To further understand the interaction mode of these compounds with S100B protein, the bound structure of the strongest-binding ligands ZINC01014143 and ZINC03307740 (with highest binding affinity from above calculation) has been examined (Fig. 8(I) and (II)) to compare with the weakest-binding ligand ZINC01743229 (with lowest binding affinity). It is noticed that the three hydrophobic rings of ligand ZINC01014143 are located in the hydrophobic pocket of the protein S100B. This indicates that hydrophobic contact may play an important role to the ligand binding. The hydrogen bonds are noticed to form between the ligand ZINC03307740 and the amino acids Glu45 and Glu46 of the protein S100B. Hydrogen bonds may have important contribution to the ligand binding. On the other hand, the ligand ZINC01743229 has three hydrophobic rings. Although two of them are located in the hydrophobic areas of the protein, the third ring is located in the hydrophilic area of the binding site. The linear shape of molecular structure of the ligand prevents the ligand from binding to the protein binding site with a favorable conformation to fit into the binding site. Hence, the hydrophobic contact surface between the ligand and the protein is not high and the binding of the ligand is weak. The ligand floats around during the simulation to locate a favorable binding configuration.

3.7. ADMET results

The absorption, distribution, metabolism, elimination and toxicity (ADMET) properties of ZINC compounds having a LUDI score of 300 or above were evaluated using ADMET predictor. This evaluation is necessary in order to save time, money, and effort in later experimentation with candidates that may be toxic or fail to pass clinical tests. As shown in Table 1, the ADMET predictor estimates the ADMET properties of ZINC compounds using eleven models. A threshold value was applied to each of the eleven

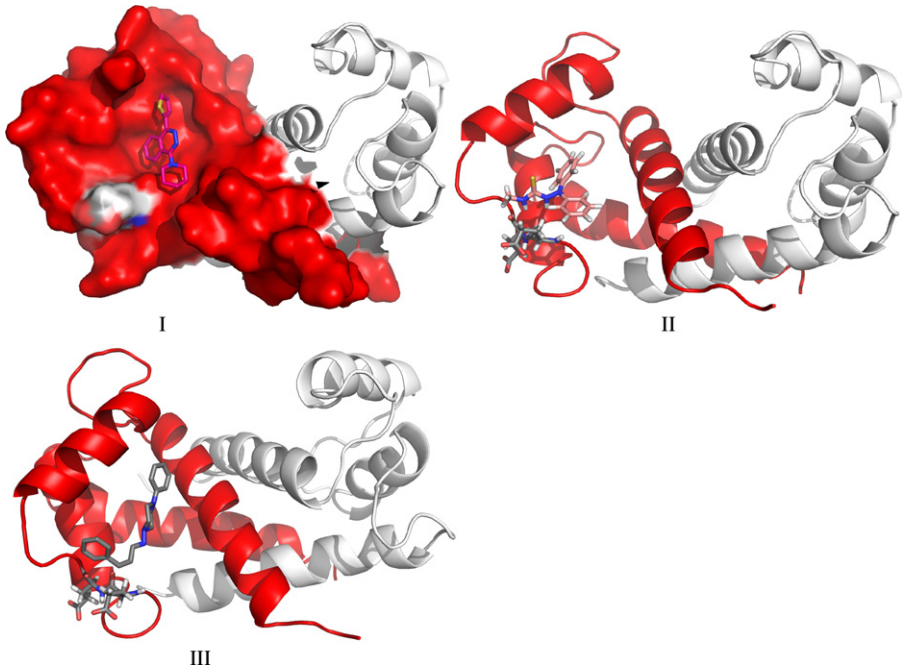

Fig. 8. The bound structures of three ligands: (I) - ligand ZINC01014143, (II) - ligand ZINC03307740, and (III) - ligand ZINC01743229. The two (ligand ZINC01014143 and ZINC03307740) with highest binding energy have better interactions than the weaker binding ligand ZINC01743229. On the bound structures, the three hydrophobic rings of ligand ZINC01014143 are located in the hydrophobic pocket of the protein S100B, which indicates the important role of hydrophobic interactions in binding. The hydrogen bonds are noticed to form between the ligand ZINC03307740 and the amino acids Glu45 and Glu46 of the S100B protein, which indicates that the hydrogen bonding has significant contributions to the ligand binding to the protein. The one monomer of S100B is shown in red.

models; and a value of "1" or "0" was assigned to each model; "1" means that the predicted values is not in the region defined by the threshold, and "0" means that the predicted value is within the region defined by the threshold. The "Admet-risk" is the summation of the results from the 11 models. Obviously, the higher the "Admet-risk" value, the more likely the compounds are toxic and can not pass the ADME test.

The prediction results are included in Table C of Supplementary materials. As can be seen from the table, few compounds have the Admet-risk value of 0, actually only three ZINC compounds in the table have an Admet-risk value of 0. In detail, most of the ZINC compounds failed in TOX-FHM prediction. More than half of the compounds have the ADMET-risk value of 1 or 2. The top-two scored compounds by LUDI score, ZINC03307740 and ZINC03257333, have the Admet-risk value of 1. The results in Table C of Supplementary materials provide valuable information to researchers who are interested in the development of these drug compounds to block the S100B–p53 interaction.

4. Conclusion

The studies on the interaction of S100B and p53 at an atomic level identified that amino acids GLU45 and GLU46 and neighboring residues are important and have important contributions to the binding of S100B with p53. A set of organic compounds that have potential to bind to S100B and block p53 from binding to S100B have been identified through a series of LUDI screenings using different searching radius. These compounds interact with S100B at the same binding sites as the C-terminal peptide of p53, and are expected to block the binding of S100B and p53. The ADME properties for the selected compounds from the screening have been predicted and the potential top compounds have been analyzed to facilitate drug development targeting the blockage of interaction of S100B and p53 proteins.

It has also been found that the LUDI algorithms seem to be fairly deterministic with consistent repeatable results, even with increasing radius. In other words, compounds found at smaller radii were retained in the search results of larger radii. The compound ZINC03307740 is ranked top in multiple LUDI screenings with radius of searching (7.23 Å, 8.23 Å and 9.23 Å, 10.23 Å).

The MMPBSA method was used to calculate the binding energies for the selected top-scored compounds from LUDI. ZINC01014143 has the highest binding affinity with a ΔG of −28.02 kcal/mol followed by ZINC03307740 with a ΔG of −27.83 kcal/mol. The distance between the center of the ligands and the center of S100B were calculated. A stronger binding energy (ΔG) was observed to be related to smaller fluctuations in distance and lower mobility of the ligands in the pocket.

Acknowledgements

This work was supported by Research Corporation Cottrell College Science Awards (CC6786), East Carolina University 2005 Research/Creativity Activity Grant, East Carolina 2007-2008 Research Development Award. YL would like to thank Simulations Plus, Inc. for performing the ADMET screening and also thank Dr. Michael B. Bolger for his advice on ADMET screening results.

Appendix A. Supplementary data

Supplementary data associated with this article can be found, in the online version, at doi:10.1016/j.jmgm.2009.02.006.

References

[1] R. Donato, S100: a multigenic family of calcium-modulated proteins of the EF-hand type with intracellular and extracellular functional roles, The International Journal of Biochemistry & Cell Biology 33 (2001) 637–668.
[2] C.W. Heizmann, Ca^{2+}-binding S100 proteins in the central nervous system, Neurochemical Research 24 (1999) 1097–1100.
[3] C.W. Heizmann, G. Fritz, B.W. Schäfer, S100 proteins: structure, function, and pathology, Frontiers in Bioscience 7 (2002) 1356–1368.
[4] J. Baudier, N. Glasser, D. Gerard, Ions binding to S100 proteins. I. Calcium- and zinc-binding properties of bovine brain S100 alpha alpha, S100a (alpha beta), and

S100b (beta beta) protein: Zn2 + regulates Ca2 + binding on S100b protein, Journal of Biological Chemistry 261 (1986) 8192–8203.
[5] K. Odink, N. Cerletti, J. Brüggen, R.G. Clerc, L. Tarcsay, G. Zwadlo, G. Gerhards, R. Schlegel, C. Sorg, Two calcium-binding proteins in infiltrate macrophages of rheumatoid arthritis, Nature 330 (1987) 80–82.
[6] R.E. Mrak, J.G. Sheng, W.S.T. Griffin, Glial cytokines in Alzheimer's disease: review and pathogenic implications, Human Pathology 26 (1995) 816–823.
[7] F. Castets, W.S.T. Griffin, A. Marks, L.J.V. Eldik, Transcriptional regulation of the human S100β gene, Molecular Brain Research 46 (1997) 208–216.
[8] J. Baudier, D. Mochly-Rosen, A. Newton, S.H. Lee, D.E. Koshland, R.D. Cole, Comparison of S100b protein with calmodulin: interactions with melittin and microtubule-associated .tau. proteins and inhibition of phosphorylation of .tau. proteins by protein kinase C, Biochemistry 26 (1987) 2886–2893.
[9] J. Baudier, R.D. Cole, Interactions between the microtubule-associated tau proteins and S100b regulate tau phosphorylation by the Ca2+/calmodulin-dependent protein kinase II, Journal of Biological Chemistry 263 (1988) 5876–5883.
[10] L.-H. Lin, L.J.V. Eldik, N. Osheroff, J.J. Norden, Inhibition of protein kinase C- and casein kinase II-mediated phosphorylation of GAP-43 by S100β, Molecular Brain Research 25 (1994) 297–304.
[11] R.R. Rust, D.M. Baldisseri, D.J. Weber, Structure of the negative regulatory domain of p53 bound to S100B(ββ), Nature Structural Biology 7 (2000) 570–574.
[12] T. Halazonetis, A. Kandil, EMBO Journal 12 (1993) 5057–5064.
[13] P. Hainaut, A. Hall, Milner, Journal of Oncogene 9 (1994) 299–303.
[14] A.J. Levine, p53, the cellular gatekeeper for growth and division, Cell 88 (1997) 323–331.
[15] M. Oren, Regulation of the p53 tumor suppressor protein, Journal of Biological Chemistry 274 (1999) 36031–36034.
[16] M.R. Fernandez-Fernandez, B. Dmitry, Veprintsev, A.R. Fersht, Proteins of the S100 family regulate the oligomerization of p53 tumor suppressor, Proceedings of the National Academy of Science USA 102 (2005) 4735–4740.
[17] M. Grigorian, S. Andresen, E. Tulchinsky, M. Kriajevska, C. Carlberg, C. Kruse, M. Cohn, N. Ambartsumian, A. Christensen, G. Selivanova, E. Lukanidin, Tumor suppressor p53 protein is a new target for the metastasis-associated Mts1/S100A4 s, Journal of Biological Chemistry 276 (2001) 22699–22708.
[18] J. Markowitz, R.R. Rustandi, K.M. Varney, P.T. Wilder, R. Udan, S.L. Wu, W.D. Horrocks, D.J. Weber, Calcium-binding properties of wild-type and ef-hand mutants of s100b in the presence and absence of a peptide derived from the C-Terminal negative regulatory domain of p53, Biochemistry 44 (2005) 7305–7314.
[19] N. Ambartsumian, M. Grigorian, I. Larsen, O. Karlstrøm, N. Sidenius, J. Rygaard, G. Georgiev, E. Lukanidin, Metastasis of mammary carcinomas in GRS/A hybrid mice transgenic for the mts1 gene, Oncogene 13 (1996) 1621–1630.
[20] M.J. Berridge, M.D. Bootman, H.L. Roderick, Calcium signalling: dynamics, homeostasis and remodelling, Nature Reviews Molecular Cell Biology 4 (2003) 517–529.
[21] B. Davies, M. Davies, F. Gibbs, R. Barraclough, P. Rudland, Induction of the metastatic phenotype by transfection of a benign rat mammary epithelial cell line with the gene for p9Ka, a rat calcium-binding protein, but not with the oncogene EJ-ras-1, Oncogene 8 (1993) 999–1008.
[22] M. Davies, P. Rudland, L. Robertson, E. Parry, P. Jolicoeur, R. Barraclough, Expression of the calcium-binding protein S100A4 (p9Ka) in MMTV-neu transgenic mice induces metastasis of mammary tumours, Oncogene 13 (1996) 1631–1637.
[23] M. Deichmann, A. Benner, M. Bock, A. Jäckel, K. Uhl, V. Waldmann, H. Näher, S100-Beta, melanoma-inhibiting activity, and lactate dehydrogenase discriminate progressive from nonprogressive american joint committee on cancer stage IV Melanoma, Journal of Clinical Oncology 17 (1999) 1891–1896.
[24] A. Ebralidze, E. Tulchinsky, M. Grigorian, A. Afanasyeva, V. Senin, E. Revazova, E. Lukanidin, Isolation and characterization of a gene specifically expressed in different metastatic cells and whose deduced gene product has a high degree of homology to a Ca2+-binding protein family, Genes Development 3 (1989) 1086–1093.
[25] A. Hauschild, J. Michaelsen, W. Brenner, P. Rudolph, R. Gläser, E. Henze, E. Christophers, Prognostic significance of serum S100B detection compared with routine blood parameters in advanced metastatic melanoma patients, Melanoma Research 9 (1999) 155–161.
[26] B.H. Lloyd, A. Platt-Higgins, P.S. Rudland, R. Barraclough, Human S100A4 (p9Ka) induces the metastatic phenotype upon benign tumour cells, Oncogene 17 (1998) 465–473.
[27] A.C. Drohat, N. TJandra, D.M. Baldisseri, D.J. Weber, The use of dipolar couplings for determining the solution structure of rat apo-S100B(ββ), Protein Science 8 (1999) 800–809.
[28] A.C. Drohat, D.M. Baldisseri, R.R. Rustandi, D.J. Weber, Solution structure of calcium-bound rat S100B(ββ) as determined by nuclear magnetic resonance spectroscopy, Biochemistry 37 (1998) 2729–2740.
[29] B.R. Brooks, R.E. Bruccoleri, B.D. Olafson, D.J. States, S. Swaminathan, M. Karplus, CHARMM: A program for macromolecular energy, minimization, and dynamics calculations, Journal Computational Chemistry 4 (1983) 187–217.
[30] A.D. MacKerell, D. Bashford, M. Bellott, R.L. Dunbrack, J.D. Evanseck, M.J. Field, S. Fischer, J. Gao, H. Guo, S. Ha, D. Joseph-McCarthy, L. Kuchnir, K. Kuczera, F.T.K. Lau, C. Mattos, S. Michnick, T. Ngo, D.T. Nguyen, B. Prodhom, W.E. Reiher, B. Roux, M. Schlenkrich, J.C. Smith, R. Stote, J. Straub, M. Watanabe, J. Wirkiewicz-Kuczera, D. Yin, M. Karplus, All-atom empirical potential for molecular modeling and dynamics studies of proteins, Journal Physical Chemistry B 102 (1988) 3586–3616.
[31] H. Böhm, The computer program LUDI: a new method for the de novo design of enzyme inhibitors, Journal of Computer Aided Molecular Design 6 (1992) 61–78.
[32] Cerius2. Retrieved from http://www.accelrys.com/products/cerius2. 2007.
[33] J.J. Irwin, B.K. Shoichet, ZINC – a free database of commercially available compounds for virtual screening, Journal of Chemical Information and Modeling 45 (2005) 177–182.
[34] W.L. Jorgensen, J. Chandrasekhar, J.D. Madura, M.L. Klein, Comparison of simple potential functions for simulating liquid water, Journal of Chemical Physics 79 (1983) 926–935.
[35] Z. Zhou, M. Khaliq, J.-E. Suk, C. Patkar, L. Li, R.J. Kuhn, C.B. Post, antiviral compounds discovered by virtual screening of small-molecule libraries against Dengue Virus E protein, ACS Chemical Biology (2008) 3.
[36] D.A. Case, T.E. Cheatham, T. Darden, H. Gohlke, R. Luo, K.M. Merz Jr., A. Onufriev, C. Simmerling, B. Wang, R.J. Woods, The Amber biomolecular simulation programs, Journal Computational Chemistry 26 (2005) 1668–1688.
[37] K. Kim, K.D. Jordan, Comparison of density functional and MP2 calculations on the water monomer and dimer, Journal Physical Chemistry 98 (1994) 10089–10094.
[38] A. Toukmaji, C. Sagui, J. Board, T. Darden, Efficient particle-mesh Ewald based approach to fixed and induced dipolar interactions, Journal Chemical Physics 113 (2000) 10913–10927.
[39] U. Essmann, L. Perera, M.L. Berkowitz, T. Darden, H. Lee, L.G. Pedersen, A smooth particle mesh Ewald method, Journal Chemical Physics 103 (1995) 8577–8593.
[40] M.F. Crowley, T.A. Darden, T.E. Cheatham III, D.W. Deerfield II, Adventures in improving the scaling and accuracy of a parallel molecular dynamics program, The Journal of Supercomputing 11 (1997) 255–278.
[41] J.-P. Ryckaert, G. Ciccotti, H.J.C. Berendsen, Numerical integration of the cartesian equations of motion of a system with constraints: molecular dynamics of n-alkanes, Journal Computational Physics 23 (1977) 327–341.
[42] J. Wang, P. Morin, W. Wang, P.A. Kollman, Use of MM-PBSA in reproducing the binding free energies to HIV-1 RT of TIBO derivatives and predicting the binding mode to HIV-1 RT of efavirenz by docking and MM-PBSA, Journal of the American Chemical Society 123 (2001) 5221–5230.
[43] W. Wang, P.A. Kollman, Free energy calculations on dimer stability of the HIV protease using molecular dynamics and a continuum solvent model, Journal of Molecular Biology 303 (2000) 567–582.
[44] P.A. Kollman, I. Massova, C. Reyes, B. Kuhn, S. Huo, L. Chong, M. Lee, T. Lee, Y. Duan, W. Wang, O. Donini, P. Cieplak, J. Srinivasan, D.A. Case, T.E. Cheatham III, Calculating structures and free energies of complex molecules: combining molecular mechanics and continuum models, Accounts of Chemical Research 33 (2000) 889–897.
[45] W. Kabsch, A solution for the best rotation to relate two sets of vectors, Acta Crystallographica A32 (1976) 922–923.
[46] C.A. Lipinski, F. Lombardo, B.W. Dominy, P.J. Feeney, Experimental and computational approaches to estimate solubility and permeability in drug discovery and development settings, Advanced Drug Delivery Reviews 23 (1997) 3–25.
[47] ADMET. Predictor v.1.0; Simulationsplus,inc: Lancaster, CA.
[48] I. Moriguchi, S. Hirono, Q. Liu, I. Nakagome, Y. Matsushita, Simple method of calculating octanol/water partition coefficient, Chem & Pharmaceutical Bulletin 40 (1992) 127–130.
[49] H. Lennernäsa, K. Palmb, U. Fagerholma, P. Arturssonb, Comparison between active and passive drug transport in human intestinal epithelial (caco-2) cells in vitro and human jejunum in vivo, International Journal of Pharmaceutics 127 (1996) 103–107.
[50] W.M. Meylan, P.H. Howard, R.S. Boethling, Improved method for estimating water solubility from octanol/water partition coefficient, Environmental Toxicology and Chemistry 15 (1996) 100–106.
[51] P. Crivori, G. Cruciani, P.-A. Carrupt, B. Testa, Predicting blood–brain barrier permeation from three-dimensional molecular structure, Journal of Medicinal Chemistry 43 (2000) 2204–2216.
[52] H. Fang, W. Tong, L.M. Shi, R. Blair, R. Perkins, W. Branham, B.S. Hass, Q. Xie, S.L. Dial, C.L. Moland, D.M. Sheehan, Structure–activity relationships for a large diverse set of natural, synthetic, and environmental estrogens, Chemical Research in Toxicology 14 (2001) 280–294.
[53] C.L. Russom, S.P. Bradbury, S.J. Broderius, D.E. Hammermeister, R.A. Drummond, Predicting modes of toxic action from chemical structure: acute toxicity in the fathead minnow (Pimephales Promealas), Environmental Toxicology and Chemistry 16 (1997) 948–967.
[54] Distributed Structure-searchable Toxicity (DSSTox) Public Database. Retrieved from http://www.epa.gov/ncct/dsstox1/5/2008.
[55] The Carcinogenic Potency Project. Retrieved from http://potency.berkeley.edu 1/7/2008.
[56] L.S. Gold, N.B. Manley, T.H. Slone, L. Rohrbach, Supplement to the carcinogenic potency database (CPDB): results of animal bioassays published in the general literature in 1993 to 1994 and by the National Toxicology Program in 1995 to 1996, Environmental Health Perspectives 107 (1999) 527–600.
[57] E.J. Matthews, N.L. Kruhlak, R.D. Benz, J.F. Contrera, Assessment of the health effects of chemicals in humans: I. QSAR estimation of the maximum recommended therapeutic dose (MRTD) and no effect level (NOEL) of organic chemicals based on clinical trial data, Current Drug Discovery Technologies 1 (2004) 61–76.